IEEE Access
Multidisciplinary | Rapid Review | Open Access Journal

Received June 8, 2020, accepted June 26, 2020, date of publication July 6, 2020, date of current version July 17, 2020.

*Digital Object Identifier 10.1109/ACCESS.2020.3007443*

# Partial Response Signaling for Circular Convolution Based Filter Bank Multi-Carrier System Adopting Quadrature Amplitude Modulation

**SEONGBAE HAN, (Graduate Student Member, IEEE), AND SOOYONG CHOI, (Member, IEEE)**
School of Electrical and Electronic Engineering, Yonsei University, Seoul 03722, South Korea

Corresponding author: Sooyong Choi (csyong@yonsei.ac.kr)

This work was supported in part by the Ministry of Science and ICT (MSIT) through the Information Technology Research Center (ITRC) Support Program supervised by the Institute for Information and Communications Technology Promotion (IITP), South Korea, under Grant IITP-2020-2018-0-01423, and in part by the National Research Foundation of Korea (NRF) funded by the Korea Government (Ministry of Science and ICT) under Grant 2017R1A2B3006025.

**ABSTRACT** A circular convolution-based filter bank multi-carrier system adopting quadrature amplitude modulation (CQAM-FBMC) that utilizes partial response signaling (PRS), referred to as the PRS-CQAM-FBMC system, is proposed and analyzed. The proposed PRS-CQAM-FBMC system has fully overlapped FBMC symbols without the time shifts and the transition time through the circular convolution filter banks in the time domain and the improved localization property by the PRS of the poorly localized QAM-FBMC symbols in the frequency domain. Therefore, the PRS-CQAM-FBMC system can achieve higher spectral efficiency than the conventional QAM-FBMC system in short-packet transmission scenarios. The analyses and simulation results show that the symbol error rate performances of the PRS-CQAM-FBMC system without cyclic prefix are robust in additive white Gaussian channels and multi-path fading channels. Moreover, the PRS-CQAM-FBMC system with the improved localization property by PRS can further provide enhanced spectral efficiency by more than 10%.

**INDEX TERMS** Circular convolution, filter bank multi-carrier (FBMC), partial response signaling (PRS), quadrature amplitude modulation (QAM).

## I. INTRODUCTION

The conventional cyclic prefix (CP)-based orthogonal frequency division multiplexing (OFDM) systems, which use CPs and guard bands, have low spectral efficiency due to CP in the time domain and very high out-of-band radiation (OoBR) in the frequency domain and are vulnerable to synchronization errors [1]. Therefore, the filter bank multi-carrier systems adopting offset quadrature amplitude modulation (OQAM-FBMC) without CP has been proposed and has received increasing attention as a new multi-carrier modulation system since they do not necessarily need the CP and can achieve higher spectral efficiency than a CP-OFDM system. That is, conventional OQAM-FBMC systems have low OoBR and are robust against synchronization errors due to per-subcarrier filtering through a well-localized prototype filter even without CP [2].

However, conventional OQAM-FBMC systems have an overhead in time domain resulting from the oversampling and overlap step in the modulation procedure, which is referred to as the transition time [3]. The transition time causes considerable loss in terms of spectral efficiency in short-packet transmission scenarios [4]. To remove the transition time, the circular convolution-based OQAM-FBMC (COQAM-FBMC) system was proposed by substituting the linear convolution in a conventional OQAM-FBMC system with a circular convolution while the localization property is severely degraded in the frequency domain [5], [6]. In addition, the conventional COQAM-FBMC cannot be used together with conventional channel estimation and multiple-input multiple-output (MIMO) techniques [1], [7].

The associate editor coordinating the review of this manuscript and approving it for publication was Faisal Tariq.

For the QAM symbol transmission, an QAM-FBMC system with two prototype filters without CP was first proposed in [7]. However, the waveform of the QAM-FBMC system in [7] is poorly localized in the frequency domain and has the transition time due the linear convolution procedure of the block-wise interleaving prototype filters. Therefore, a circular convolution-based filter bank multi-carrier system adopting quadrature amplitude modulation (CQAM-FBMC) that utilizes partial response signaling (PRS), referred to as the PRS-CQAM-FBMC system, is proposed and analyzed.

To remove the transition time of the conventional QAM-FBMC system, we adopt the circular convolution procedure to the conventional QAM-FBMC system as in [5], [6] and obtain the fully overlapped FBMC symbols without time shifts and the transition time. Subsequently, we apply the PRS techniques to improve the degraded localization property caused by the fully overlapped symbol from the circular convolution procedure and the block-wise interleaving prototype filters. That is, the PRS procedure performed on multiple subcarriers in the frequency domain shapes the poorly localized waveform into a well-localized one and provides a lower OoBR without CP. Therefore, the proposed PRS-QAM-FBMC system can transmit the QAM symbols along with the conventional channel estimation and MIMO techniques and provide higher spectral efficiency without CP and guard band.

## II. CONVENTIONAL QAM-FBMC SYSTEM

The conventional QAM-FBMC system in [7] with $M$ subcarriers is considered. Suppose that the $M$ QAM symbols are modulated in a multi-carrier symbol using $M$ subcarriers. We call the multi-carrier modulated symbol an FBMC symbol. In a QAM-FBMC system, the $M$ QAM symbols on an FBMC symbol are divided into two groups. One group is modulated on the even-numbered subcarriers, and the other group is modulated on the odd-numbered subcarriers. Each of the $M$ QAM symbols are modulated on the $(2s + b)$-th subcarrier, where $b \in \{0, 1\}$ and $s \in \{0, 1, \ldots, M/2 - 1\}$. The two prototype filters $g_0$ and $g_1$ are used to modulate the first and second QAM symbol groups, respectively. Each of the two prototype filters has $KM$ coefficients, that is, $g_b = [g_b[0], g_b[1], \ldots, g_b[KM - 1]]$, where $K$ is called an oversampling factor, and $\sum_{i=0}^{KM-1} |g_b[i]|^2 = 1$. The discrete time transmit signal $s[i]$ of the QAM-FBMC systems can be expressed as

$$s[i] = \sum_{n\in\mathbf{Z}} \sum_{b=0}^{1} \sum_{s=0}^{M/2-1} a_{b,s}^{n} g_{b,s}^{n}[i], \tag{1}$$

where $i$ is a sample index on the time domain, $\mathbf{Z}$ denotes the set of integers, and $g_{b,s}^{n}[i]$ are shifted versions of $g_b[i]$ by $nM$ samples in the time domain and $2s$ subcarriers in the frequency domain. $g_{b,s}^{n}[i]$ is given by

$$g_{b,s}^{n}[i] = g_b\,[i - nM]\, e^{j\frac{2\pi}{M}(2s+b)i}. \tag{2}$$

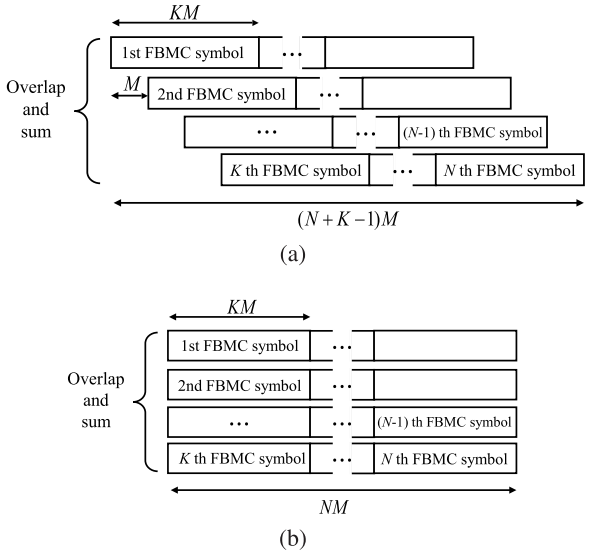


**FIGURE 1. Signal representation for the overlap and sum process: (a) QAM-FBMC system, and (b) CQAM-FBMC system.**

For orthogonal transmission and reception, two prototype filters should satisfy the orthogonality conditions explained in [7], as follows:

$$\sum_{i=-\infty}^{\infty} g_{b,s}^{n}[i] g_{b',s'}^{n'*}[i] = \delta_{n,n'}\delta_{b,b'}\delta_{s,s'}, \tag{3}$$

where $\delta_{x,x'}$ denotes the Kronecker delta. To satisfy conditions (3), a block-wise interleaving filter was proposed in [7]. However, with block-wise interleaving, discontinuous points arise at an interval of $M/2$ samples in the impulse response of the filter. The discontinuous points degrade the localization property in the frequency domain, and the OoBR increases. In addition, the length of the transmit signal becomes longer due to oversampling and overlap in the modulation procedure, as shown in Fig. 1(a). The length of FBMC symbol is $KM$ samples, which is $L$ times longer than that of OFDM symbol due to oversampling. There is also a time shift of $M$ samples between consecutive FBMC symbols. Therefore, $(N + K - 1)\,M$ samples are needed to transmit $N$ FBMC symbols. While the OFDM system without the CP requires $NM$ samples to transmit $N$ OFDM symbols, the QAM-FBMC system needs $(K - 1)\,M$ samples more than the OFDM system. The additional $(K - 1)\,M$ samples, together known as the transition time, are not a trivial overhead when $N$ is small.

## III. CIRCULAR CONVOLUTION-BASED QAM-FBMC SYSTEM UTILIZING PARTIAL RESPONSE SIGNALING

This section introduces the proposed PRS-CQAM-FBMC system to improve the spectral efficiency of the conventional QAM-FBMC system in the time and frequency domains. The proposed PRS-CQAM-FBMC system can be obtained by the following two steps. First, we obtain the CQAM-FBMC from a conventional QAM-FBMC system to eliminate the transition time in the time domain. Then, the proposed

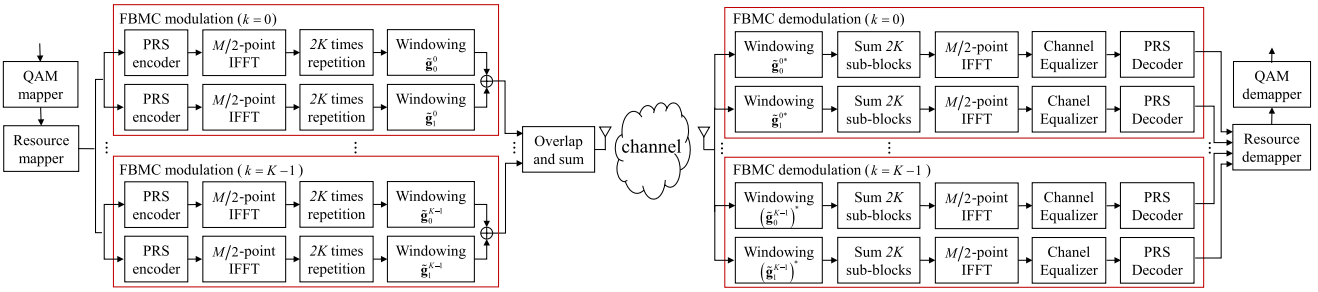


**FIGURE 2.** Block diagram of the transmitter and receiver in a PRS-CQAM-FBMC system.

PRS-CQAM-FBMC system can be obtained from the CQAM-FBMC system to improve the localization property of the waveforms in the frequency domain. We apply the circular convolution procedure to the conventional QAM-FBMC system to remove the transition time instead of the linear convolution procedure as in [5]. The transmit signal of the CQAM-FBMC system can be expressed as

$$s[i] = \sum_{n\in\mathbf{Z}} \sum_{b=0}^{1} \sum_{s=0}^{M/2-1} a_{b,s}^{n} \tilde{g}_{b,s}^{n}[i]. \tag{4}$$

$\tilde{g}_{b,s}^{n}[i]$ is given by

$$\tilde{g}_{b,s}^{n}[i] = \hat{g}_{b}^{k}\left[i - \left\lfloor \frac{n}{K} \right\rfloor KM\right] e^{j\frac{2\pi}{M}(2s+b)i}, \tag{5}$$

where $\lfloor . \rfloor$ denotes floor function. $\hat{g}_{b}^{k}[i]$ is obtained by circularly shifting the prototype filter $g_b[i]$ as $kM$ samples in the time domain, where $k = \mathrm{mod}(n, K)$, which means $n$ modulo $K$ operation. Therefore, $\hat{g}_{b}^{k}[i]$ can be expressed as

$$\hat{g}_{b}^{k}[i] \triangleq \begin{cases} g_b\left[\mathrm{mod}(i - kM, KM)\right], & 0 \le i \le KM \\ 0, & otherwise. \end{cases} \tag{6}$$

As shown in Fig. 1(b), $K$ FBMC symbols are fully overlapped in a one block interval of $KM$ samples without the time shift, and the transition time can be removed. Therefore, the CQAM-FBMC system requires $\lceil \frac{N}{K} \rceil KM$ samples to transmit $N$ CQAM-FBMC symbols, where $\lceil . \rceil$ denotes ceiling function.

In one block interval, $\hat{g}_{b}^{k}[i]$ is generated as $K$ circularly shifted versions for each of the two prototype filters, $g_0$ and $g_1$. Therefore, $2K$ filters are used in each block interval. Unfortunately, the circular shift leads to discontinuous points at both edges of $\hat{g}_{b}^{k}[i]$, which degrades the localization property of $\hat{g}_{b}^{k}[i]$. Thus, to improve the localization property, we apply the PRS procedure selectively on multiple subcarriers in the frequency domain to the CQAM-FBMC system and obtain the proposed PRS-CQAM-FBMC system.

Fig. 2 shows the block diagram of the transmitter and receiver in the PRS-CQAM-FBMC system. The PRS encoder is added before the $M/2$-point inverse discrete Fourier transform (IDFT). The PRS operation is selectively performed to the QAM symbols and not to every QAM symbols. Let the vector $\mathbf{a}_b^n$ be a group of $M/2$ QAM symbols modulated on

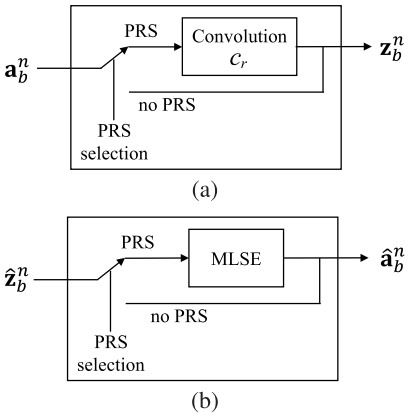


**FIGURE 3.** Block diagram of the PRS encoder and decoder in a PRS-CQAM-FBMC system: (a) PRS encoder and (b) PRS decoder.

the $n$-th FBMC symbol using the $b$-th prototype filter. That is, $\mathbf{a}_b^n = [a_{b,0}^n, a_{b,1}^n, \ldots, a_{b,M/2-1}^n]$. The output of the PRS encoder for $\mathbf{a}_b^n$ is denoted as $\mathbf{z}_b^n = [z_{b,0}^n, z_{b,1}^n, \ldots, z_{b,M/2-1}^n]$. The PRS encoder determines whether the PRS procedure is conducted onto $\mathbf{a}_b^n$, and the PRS procedure is then applied to the selected $\mathbf{a}_b^n$, as shown in Fig. 3(a). This PRS procedure is applied using the discrete convolution between $\mathbf{a}_b^n$ and the partial response (PR) coefficients as in [8], [9]. Therefore, $z_{b,s}^n$ can be expressed as

$$z_{b,s}^{n} = \begin{cases} a_{b,\,s}^{n} & \text{if PRS is not applied} \\ \sum_{r=0}^{L-1} c_r a_{b,\,\mathrm{mod}\,(s-r,M/2)}^{n} & \text{if PRS is applied,} \end{cases} \tag{7}$$

where $c_r$ denotes the $r$-th PR coefficient and $L$ denotes the length of PR coefficients, i.e., $\mathbf{c} = \{c_0, c_1, \ldots, c_{L-1}\}$. Then, the transmit signals of the PRS-CQAM-FBMC system can be obtained by replacing $a_{b,s}^n$ with $z_{b,s}^n$ in (4). Therefore, the transmit signal of the PRS-CQAM-FBMC system, $s_{prs-cqam}[i]$, can be expressed as

$$s_{prs-cqam}[i] = \sum_{n\in\mathbf{Z}} \sum_{b=0}^{1} \sum_{s=0}^{M/2-1} z_{b,s}^{n} \tilde{g}_{b,s}^{n}[i] \tag{8}$$

$$= \sum_{n\in\mathbf{Z}} \sum_{b=0}^{1} \hat{g}_{b}^{k}\left[i - \left\lfloor \frac{n}{K} \right\rfloor KM\right] e^{j\frac{2\pi b}{M}i} Z_b^n[i], \tag{9}$$

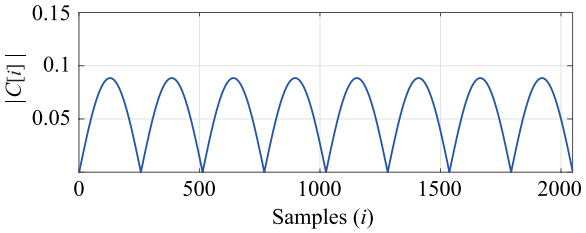


**FIGURE 4.** $C[i]$, where $0 \le i \le KM-1$. Number of subcarriers $M = 512$ and overlapping factor $K = 4$.

where $Z_b^n[i] = \sum_{s=0}^{M/2-1} z_{b,s}^n e^{j\frac{2\pi s}{M/2}i}$. If the PRS procedure is applied to $\mathbf{a}_b^n$ in (7), $Z_b^n[i]$ can be written as

$$Z_b^n[i] = \sum_{s=0}^{M/2-1}\sum_{r=0}^{L-1} c_r a_{b,\ \mathrm{mod}\ (s-r,M/2)}^n e^{j\frac{2\pi s}{M/2}i} \tag{10}$$

$$= C[i]\sum_{s=0}^{M/2-1} a_{b,\,s}^n e^{j\frac{2\pi s}{M/2}i}, \tag{11}$$

where $C[i]$ is the $M/2$-point IDFT output of $\mathbf{c}$ and is written as $C[i] = \sum_{r=0}^{L-1} c_r e^{j\frac{2\pi r}{M/2}i}$. In (11), the IDFT output of $\mathbf{a}_b^n$ is windowed by $C[i]$ in the time domain. Fig. 4 shows the absolute values of $C[i]$, which has null points at $i = 0, M/2, M, \ldots, KM$, when we used $\{\frac{1}{\sqrt{2}}, -\frac{1}{\sqrt{2}}\}$ as the PRS coefficients as an example in this paper. As the IDFT output of $\mathbf{a}_b^n$ is windowed by $C[i]$ in the proposed scheme, the null points can suppress the envelope of the discontinuous points owing to the block-wise interleaving and the circular convolution procedure. Therefore, the localization property of the transmit signals in the time and frequency domains can be improved.

In the proposed scheme, the PRS encoder is selectively applied to some poorly localized FBMC symbols. Therefore, a criterion is required to select FBMC symbols and decide whether the PRS encoder should be applied to each data symbol group. As the waveform of each FBMC symbol depends on $\tilde{g}_{b,0}^n[i]$, the proposed scheme selects the FBMC symbols to apply the PRS procedure based on the localization property of the baseband filters, $\tilde{g}_{b,0}^n[i]$. Thus, $2K$ baseband filters are ordered according to the localization property of each baseband filter, and $N_p$ poorly localized baseband filters are selected. Subsequently, the proposed scheme applies the PRS procedure to the FBMC symbols corresponding to the $N_p$ baseband filters. To measure the quality of the localization property, we define $\gamma(\Delta f, g)$ as the energy ratio in the frequency range $-\Delta f \le f \le \Delta f$, and can be written as

$$\gamma(\Delta f, g) = \frac{\int_{-\Delta f}^{\Delta f} \left|G\left(e^{j2\pi f}\right)\right|^2 df}{\int_{-\infty}^{\infty} \left|G\left(e^{j2\pi f}\right)\right|^2 df}, \tag{12}$$

where $G\left(e^{j2\pi f}\right)$ is the Fourier transform of $g[i]$. We then calculate $\Delta f$ for a fixed energy ratio $\eta$ and $g[i]$ (i.e., $\Delta f(\eta, g) = \gamma^{-1}(\eta, g)$). $\Delta f$ can show how dispersive the energy of the filter is in the frequency domain. $\Delta f$ is calculated for each baseband filter, following which all baseband filters are sorted in the ascending order of $\Delta f$. Then, we select $N_p$ baseband filters corresponding to bigger $\Delta f$.

On the other hand, an additional step is required to decode the PRS symbols and compensate for the ICI after the filter bank at the receiver, since the PRS procedure induces ICI [9]. In the proposed scheme, a maximum likelihood sequence equalization (MLSE) using the Viterbi algorithm is adopted to decode the PRS symbols, as shown in Figs. 2 and 3(b). Therefore, the computational complexity at the receiver increases due to the added PRS decoding process. When the $J^2$-ary QAM and $M_d$ subcarriers are used for data transmission, the computational complexity of the Viterbi algorithm is $O(J^{2(L-1)}M_d)$. The length of the output of the PRS encoder $\mathbf{z}_b^n$ is longer than the input data sequence $\mathbf{a}_b^n$ by $L-1$ due to the linear convolution with PR coefficients at the PRS encoder. Since there are two QAM symbol groups corresponding to two prototype filters, the proposed scheme requires $2(L-1)$ more subcarriers than the conventional FBMC systems. Therefore, the PR coefficients with a large value of $L$ would not be preferred to reduce the computational complexity and increase spectral efficiency. In this paper, the length of PR coefficients is 2. Consequently, the computational complexity of the Viterbi algorithm becomes $O(J^2M_d)$ and linearly increases in proportion to the modulation order $J^2$ and the number of used subcarriers $M_d$. In addition, only two subcarriers are more required.

## IV. ERROR PROBABILITY ANALYSIS

In this section, we analyze the symbol error rate (SER) of the PRS-CQAM-FBMC system in the additive white Gaussian noise (AWGN) channel based on the asymptotic SER of the PRS decoding for pulse amplitude modulation (PAM) [10] and analysis of SERs for PAM and QAM in AWGN channel [11].

When the received signal in frequency domain for the $n$-th FBMC symbol using the $b$-th prototype filter is given by $\mathbf{r}_b^n = [r_{b,0}^n, r_{b,1}^n, \ldots, r_{r,M/2-1}^n]$, $r_{b,s}^n$ can be expressed as

$$r_{b,s}^n = z_{b,s}^n + w_{b,s}^n, \tag{13}$$

where $w_{b,s}^n$ denotes the AWGN sample that is an independent and identically distributed (i.i.d.) circularly symmetric complex Gaussian random variable with zero mean and variance of $\sigma_n^2$. Moreover, the average symbol power is denoted by $E_s$, i.e., $\mathbb{E}[|z_{b,s}^n|^2] = E_s$.

If the PRS procedure is applied, $z_{b,s}^n$ is the PRS encoded $J^2$-ary QAM symbol. The Viterbi algorithm is used to decode the PRS encoded symbols at the PRS decoder and operates for the in-phase and quadrature channels separately. Therefore, $r_{b,s}^n$ can be divided into the in-phase and quadrature components denoted as $\mathbb{R}\{r_{b,s}^n\}$ and $\mathbb{I}\{r_{b,s}^n\}$, which are expressed as

$$\mathbb{R}\{r_{b,s}^n\} = \mathbb{R}\{z_{b,s}^n\} + \mathbb{R}\{w_{b,s}^n\}, \tag{14}$$

$$\mathbb{I}\{r_{b,s}^n\} = \mathbb{I}\{z_{b,s}^n\} + \mathbb{I}\{w_{b,s}^n\}, \tag{15}$$

respectively. $\mathbb{R}\{z^n_{b,s}\}$ and $\mathbb{I}\{z^n_{b,s}\}$ can be considered as the PRS encoded $J$-ary PAM symbols and $\mathbb{E}[|\mathbb{R}\{z^n_{b,s}\}|^2] = \mathbb{E}[|\mathbb{I}\{z^n_{b,s}\}|^2] = \frac{E_s}{2}$. Since the variance of $\mathbb{R}\{w^n_{b,s}\}$ and $\mathbb{I}\{w^n_{b,s}\}$ is $\frac{\sigma_n^2}{2}$, the SER of in-phase component is the same as that of quadrature component.

When $J$-ary PAM is used, the asymptotic SER of Viterbi algorithm for the PRS decoding at a high signal-to-noise ratio (SNR) is given by

$$P_{prs,PAM} = 4(J-1)Q\left(\sqrt{\frac{3E_s}{(J^2-1)\sigma_n^2}}\right). \tag{16}$$

The SER of the PRS encoded $J^2$-ary QAM symbol can be calculated by the SERs of in-phase and quadrature components and expressed as

$$P_{prs,QAM} = 1-(1-P_{prs,PAM})^2. \tag{17}$$

If PRS is not applied, $z^n_{b,s}$ is $J^2$-ary QAM symbol. Hence, the SER of $J^2$-ary QAM symbol in AWGN channel, which is denoted by $P_{QAM}$, is given by

$$P_{QAM} = 1-\left(1-\frac{2(J-1)}{J}Q\left(\sqrt{\frac{3E_s}{(J^2-1)\sigma_n^2}}\right)\right)^2. \tag{18}$$

Therefore, since the PRS-CQAM-FBMC system selectively applies the PRS procedure to $N_p$ FBMC symbols out of $2K$ FBMC symbols in one block interval, the SER of PRS-CQAM-FBMC system can be expressed as

$$P_{prs-cqam} = \frac{1}{2K}(N_pP_{prs,QAM} + (2K-N_p)P_{QAM}). \tag{19}$$

## V. SPECTRAL EFFICIENCY ANALYSIS

To analyze spectral efficiency, the Gabor system is utilized as in [12]. The lattice density of the Gabor system represents the density of the QAM symbols in the time–frequency domain and can be expressed as

$$\frac{N_{sym}}{T_0 \cdot B_0}, \tag{20}$$

where $T_0$ denotes the transmission time, $B_0$ denotes the bandwidth of the multi-carrier system, and $N_{sym}$ is the number of QAM symbols for $T_0$ and $B_0$.

Suppose that $N$ FBMC symbols are transmitted, and $M_d$ subcarriers with a size of over $M$-point FFT are used to transmit the information symbols. Therefore, $N_{sym} = NM_d$. When the subcarrier spacing is $F_0$, the sampling duration $T_s$ is $1/MF_0$. The conventional QAM-FBMC system needs a guard band $B_g$ to supplement the poorly localized spectrum. Therefore, the total bandwidth of the conventional QAM-FBMC system, $B_{0,qamfbmc}$, is $M_dF_0 + B_g$. The transmit time of the conventional QAM-FBMC system for $N_{sym}$ symbols, $T_{0,qamfbmc}$, is $((N+K-1)MT_s)$ as shown in Fig. 1(a). By replacing $T_0$ and $B_0$ in (20) with $T_{0,qamfbmc}$ and $B_{0,qamfbmc}$, respectively, the lattice density of the conventional QAM-FBMC system, $\eta_{qamfbmc}$, is given by

$$\eta_{qamfbmc} = \frac{NM_d}{((N+K-1)MT_s)\cdot(M_dF_0+B_g)}. \tag{21}$$

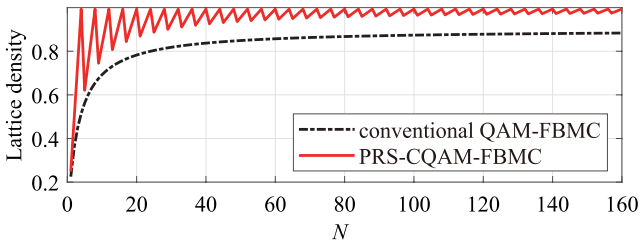


**FIGURE 5.** Lattice densities of the conventional QAM-FBMC and PRS-CQAM-FBMC systems.

**TABLE 1.** Ratio between lattice densities of the PRS-CQAM-FBMC and conventional QAM-FBMC systems.

| $N$ | 20 | 80 | 160 |
|---|---|---|---|
| $\eta_{qamfbmc}$ | 0.7826 | 0.8675 | 0.8834 |
| $\eta_{prscqam}$ | 0.9934 | 0.9934 | 0.9934 |
| $\frac{\eta_{prscqam}}{\eta_{qamfbmc}}$ | 126.94 % | 114.51 % | 112.45 % |

Since the PRS procedure makes the spectrum of the PRS-CQAM-FBMC system well-localized, a guard band $B_g$ is not needed. However, the PRS encoding requires the $2(L-1)$ additional subcarriers. Therefore, the total bandwidth of the PRS-CQAM-FBMC system, $B_{0,prscqam}$, is $(M_d + 2(L-1))F_0$. In addition, the transmission time is reduced by the circular convolution procedure and the transmission time for $N_{sym}$ symbols, $T_{0,prscqam}$, is $\lceil \frac{N}{K} \rceil KM$. By replacing $T_0$ and $B_0$ in (20) with $T_{0,prscqam}$ and $B_{0,prscqam}$, the lattice density of the PRS-CQAM-FBMC system, $\eta_{prscqam}$, is

$$\eta_{prscqam} = \frac{NM_d}{\left(\lceil \frac{N}{K} \rceil KMT_s\right)\cdot((M_d+2(L-1))F_0)}. \tag{22}$$

Fig. 5 shows the lattice density of the conventional FBMC-QAM and PRS-CQAM-FBMC systems when $F_0 = 15$ kHz, $M = 300$, $K = 4$, and $B_g = 0.5$ MHz. Table 1 shows the ratio between lattice densities of the PRS-CQAM-FBMC and conventional QAM-FBMC systems, which is defined as $\frac{\eta_{prscqam}}{\eta_{qamfbmc}}$. The PRS-CQAM-FBMC system shows the improved lattice densities compared with the conventional QAM-FBMC system. If $N$ is a multiple of $K$, the PRS-CQAM-FBMC system maintains a high lattice density when $N$ is small. Therefore, the PRS-CQAM-FBMC system can achieve a much higher lattice density than the conventional QAM-FBMC system owing to the reduced transmission time in short-packet transmission scenarios. Even though the packet length is long, the PRS-CQAM-FBMC system can achieve higher lattice density than the conventional QAM-FBMC system, since the PRS-CQAM-FBMC system does not require the guard band in the frequency domain.

## VI. SIMULATION RESULTS

In this section, the performances in terms of SER and the power spectral density (PSD) of the proposed

**TABLE 2. Simulation parameters.**

| Parameter | Value |
|---|---|
| FFT/IFFT size ($M$) | 512 |
| Number of subcarriers ($M_d$) | 300 |
| Subcarrier spacing ($F_0$) | 15 kHz |
| Center frequency | 2 GHz |
| Modulation | 4-QAM |
| Overlapping factor ($K$) | 4 |
| Threshold for filter selection ($\gamma$) | 0.95 |

PRS-QAM-FBMC system are compared with those of the conventional QAM-FBMC system in [7]. The simulation parameters are presented in Table 2. The number of subcarriers and subcarrier spacing are set as those in LTE system with a 5-MHz bandwidth [13]. Perfect channel estimation and time–frequency synchronization are assumed. The PHYDYAS prototype filter in [3] with $K = 4$ is used for $\mathbf{g}_0$. $\mathbf{g}_1$ is generated from $\mathbf{g}_0$ as the prototype filter for the odd-numbered subcarriers in [7].

Fig. 6 shows the SERs for the conventional QAM-FBMC, CQAM-FBMC, and PRS-CQAM-FBMC systems in AWGN channel. Lines and Markers in Fig. 6 show the analytical results and Monte Carlo simulation results, respectively. The analytical results are well matched to the simulation results at the high SNRs above 11dB. As the conventional QAM-FBMC and CQAM-FBMC systems satisfy the orthogonality condition, there is no intrinsic interference. Therefore, the SERs of the conventional QAM-FBMC and CQAM-FBMC systems are the same as $P_{QAM}$. Otherwise, the SERs of the PRS-CQAM-FBMC systems degrade as $N_p$ increases due to the ICI caused by the PRS. The SERs of the PRS-CQAM-FBMC system are also lower compared with those of the CQAM-FBMC system, since the SNR loss of the PRS-FBMC-CQAM system increases as $N_p$ increases.

Fig. 7 shows the SERs of the conventional QAM-FBMC, CQAM-FBMC, and PRS-CQAM-FBMC systems in a multi-path fading channel. The power delay profile of the ITU-R vehicular-A channel model in [14] is used. In the low SNR region, the SERs of the PRS-CQAM-FBMC systems are degraded due to the PRS, similar to the case of the SERs in the AWGN channel. However, in the high SNR region, the SERs of the PRS-CQAM-FBMC systems are improved as $N_p$ increases. The interference caused by multi-path fading is reduced by the PRS. When $N_p$ exceeds 5, the SERs of the PRS-CQAM-FBMC system is sufficiently robust against a multi-path fading channel. Although the SERs of PRS-CQAM-FBMC systems is slightly lower than those of conventional QAM-FBMC systems, the PRS-CAM-FBMC system can achieve higher spectral efficiency than the conventional QAM-FBMC system.

Fig. 8 shows the PSDs of the conventional QAM-FBMC, CQAM-FBMC, and PRS-CQAM-FBMC systems. The OoBR of the PRS-CQAM-FBMC system decreases as $N_p$ increases. When $N_p$ exceeds 5, the OoBR of the PRS-CQAM-FBMC system is much lower than those of the conventional QAM-FBMC and CQAM-FBMC systems.

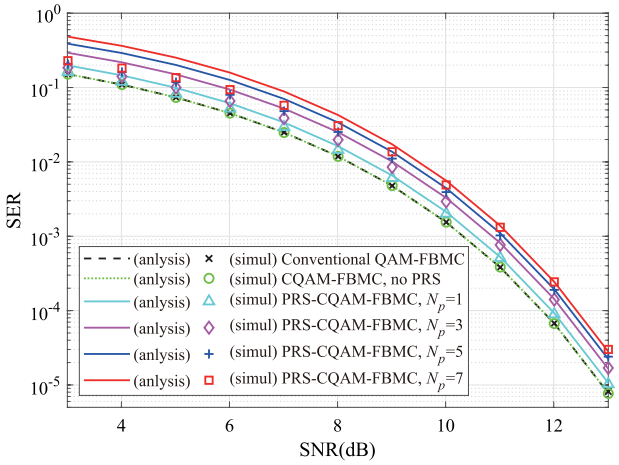


**FIGURE 6. SERs of the conventional QAM-FBMC, CQAM-FBMC, and PRS-CQAM-FBMC systems for 4-QAM in the AWGN channel.**

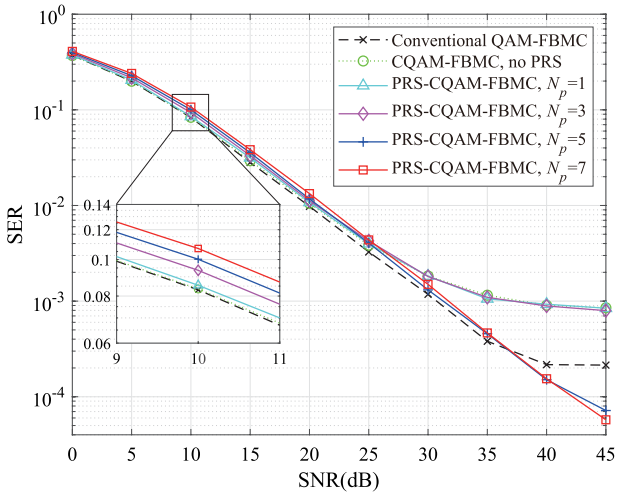


**FIGURE 7. SERs of the conventional QAM-FBMC, CQAM-FBMC, and PRS-CQAM-FBMC systems for 4-QAM in a multi-path fading channel.**

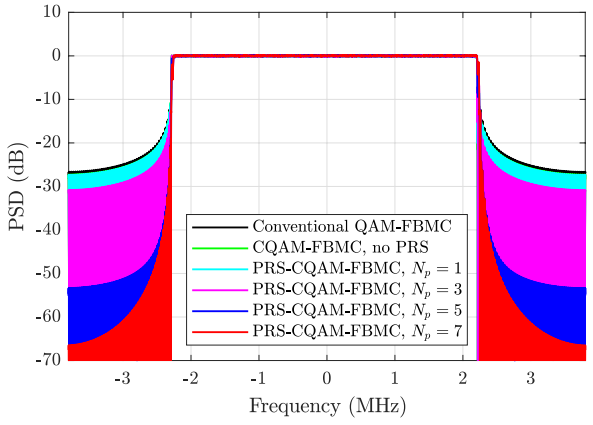


**FIGURE 8. PSDs of the conventional QAM-FBMC, CQAM-FBMC, and PRS-CQAM-FBMC systems.**

## VII. CONCLUSION

In this paper, we proposed the PRS-CQAM-FBMC system with the fully overlapped FBMC symbols without the time shifts and the transition time by the circular convolution filter banks in the time domain and by the PRS procedure of QAM symbols on multiple subcarriers in the frequency domain. The simulation results showed that the proposed PRS-QAM-FBMC system without CP and guard band has a higher spectral efficiency as well as the better SER and PSD performances than the conventional QAM-FBMC and CQAM-FBMC systems due to the improved localization property from the PRS procedure. The proposed scheme is a potentially alternative way to obtain well-localized waveforms in future multi-carrier modulation systems.

## REFERENCES

[1] C. Kim, Y. H. Yun, K. Kim, and J.-Y. Seol, "Introduction to QAM-FBMC: From waveform optimization to system design," *IEEE Commun. Mag.*, vol. 54, no. 11, pp. 66–73, Nov. 2016.

[2] B. Farhang-Boroujeny, "OFDM versus filter bank multicarrier," *IEEE Signal Process. Mag.*, vol. 28, no. 3, pp. 92–112, May 2011.

[3] M. Bellanger, "FBMC physical layer: A primer," PHYDYAS FP7 Project, Paris, France, Tech. Rep., Jan. 2010. [Online]. Available: http://www.ict-phydyas.org/teamspace/internal-folder/FBMC-Primer_06-2010.pdf

[4] F. Schaich, T. Wild, and Y. Chen, "Waveform contenders for 5G–suitability for short packet and low latency transmissions," in *Proc. IEEE 79th Veh. Technol. Conf. (VTC Spring)*, Seoul, South Korea, May 2014, pp. 1–5.

[5] H. Lin and P. Siohan, "Multi-carrier modulation analysis and WCP-COQAM proposal," *EURASIP J. Adv. Signal Process.*, vol. 2014, no. 1, p. 79, Dec. 2014.

[6] M. J. Abdoli, M. Jia, and J. Ma, "Weighted circularly convolved filtering in OFDM/OQAM," in *Proc. IEEE 24th Annu. Int. Symp. Pers., Indoor, Mobile Radio Commun. (PIMRC)*, London, U.K., Sep. 2013, pp. 657–661.

[7] H. Nam, M. Choi, S. Han, C. Kim, S. Choi, and D. Hong, "A new filter-bank multicarrier system with two prototype filters for QAM symbols transmission and reception," *IEEE Trans. Wireless Commun.*, vol. 15, no. 9, pp. 5998–6009, Sep. 2016.

[8] A. Lender, "The duobinary technique for high-speed data transmission," *IEEE Trans. Commun. Electron.*, vol. CE-82, no. 2, pp. 214–218, May 1963.

[9] P. Kabal and S. Pasupathy, "Partial-response signaling," *IEEE Trans. Commun.*, vol. COM-23, no. 9, pp. 921–934, Sep. 1975.

[10] H. Kobayashi, "Correlative level coding and maximum-likelihood decoding," *IEEE Trans. Inf. Theory*, vol. IT-17, no. 5, pp. 586–594, Sep. 1971.

[11] A. Goldsmith, *Wireless Communications*. Cambridge, U.K.: Cambridge Univ. Press, 2005.

[12] A. Sahin, I. Guvenc, and H. Arslan, "A survey on multicarrier communications: Prototype filters, lattice structures, and implementation aspects," *IEEE Commun. Surveys Tuts.*, vol. 16, no. 3, pp. 1312–1338, 3rd Quart., 2014.

[13] E. Dahlman, S. Parkvall, and J. Sköld, *4G: LTE/LTE-Advanced for Mobile Broadband*. New York, NY, USA: Academic, 2011.

[14] N. Chayat, *Tentative Criteria for Comparison of Modulation Methods*, document IEEE P802.11-97-96, Sep. 1999.

**SEONGBAE HAN** (Graduate Student Member, IEEE) received the B.S. degree in electrical and electronic engineering from Yonsei University, Seoul, South Korea, in 2014, where he is currently pursuing the Ph.D. degree. His research interests include new waveforms, multicarrier modulation schemes, massive multiple-input multiple-output systems, and machine learning-based wireless communication systems.

**SOOYONG CHOI** (Member, IEEE) was born in Seoul, South Korea, in 1971. He received the B.S.E.E., M.S.E.E., and Ph.D. degrees from Yonsei University, Seoul, in 1995, 1997, and 2001, respectively. In 2001, he was a Postdoctoral Researcher with the IT Research Group, Yonsei University. His work focused on proposing and planning for the fourth generation communication systems. From 2002 to 2004, he was a Postdoctoral Fellow with the University of California at San Diego, La Jolla, CA, USA. From 2004 to 2005, he was a Researcher with Oklahoma State University, Stillwater, OK, USA. From 2005 to 2016, he was an Assistant Professor and an Associate Professor with the School of Electrical and Electronic Engineering, Yonsei University, where he has been a Professor, since 2016. His research interests include adaptive signal processing techniques (equalization and detection), massive multiple-input multiple-output systems for wireless communication, and new waveforms and multicarrier transmission techniques for future wireless communication systems.